A Primer for the use of Satellite Imagery in Geologic Investigations

James S. Chapman, PG

North Carolina Geological Survey
Open-File Report 2020-01

29 May 2020

Suggested citation: Chapman, James S., 2020, A Primer for the use of Satellite Imagery in Geologic Investigations, North Carolina Geological Survey, Open File Report 2020-01, 45 pages.

CONTENTS

ABSTRACT

Satellite imagery has been used for geological investigations since the first Earth observation satellites were first launched. In 1972, the United Stated began a long line of satellites with the Landsat missions (Landsat 8 being the latest to date). The European Union established the Sentinel-2 Earth observation mission for optical imaging with a two satellite constellation, the first satellite launched in 2015 followed by the second one in 2017. The Landsat and Sentinel missions provide a vast amount of easily accessible land imagery scenes, delivered as separate spectral band wavelength files. The spectral bands can be combined and transformed with different techniques to highlight material reflectance features, which can then be used to identify potential mineral or land textural features for identification and mapping purposes.

This report summarizes some of the most used current techniques for manipulating the spectral bands, with an emphasis on geology investigations. Although change through short time differentials is crucial for geological hazards investigations, this primer report is mainly concerned with investigations in material identification. Light wavelength and radiance (spectral resolution and radiometric resolution, respectively) are the light parameters that the analyst works with and, when combined with spatial resolution (minimum area detection), material content and/or texture present signatures for identification use. In the post-processing, further image manipulation, such as pansharpening, contrast stretching, and targeted filtering techniques also aid in identifying material at the Earth's surface for light reflectance qualities.

Satellite image analysis, combined with a working geological knowledge of the area of interest, can be a powerful and robust tool for future geology investigation analysis work. Geology investigations will increasingly use remote sensing tools (i.e.; satellite spectral imagery, synthetic aperture radar, and light detection and ranging) in combination with in situ field work to enhance understanding.

GLOSSARY

digital number (DN) - generic term for pixel values. It is commonly used to describe pixel values that have not yet been calibrated into physically meaningful units. It is a relative radiometric intensity (brightness) value assigned to a pixel.

Earth observation (EO) - The gathering of information about Earth's physical, chemical and biological systems. It involves monitoring and assessing the status of, and changes in, the natural and man-made environment.

electromagnetic radiation (EMR) - A form of energy that is produced by oscillating electric and magnetic disturbance, or by the movement of electrically charged particles traveling through a vacuum or matter (**Tipler, 1999**). Light, electricity, and magnetism are all different forms of electromagnetic radiation.

Environmental Systems Research Institute (ESRI) - An international supplier of geographic information system (GIS) software, web GIS, and geodatabase management applications.

European Space Agency (ESA) – Established in 1975 and headquartered in Paris, France, the organization has 22 member states dedicated to the exploration of space (**ESA, 2020**).

field-of-view (FOV) - The maximum angle of view which a passive electromagnetic sensor can effectively detect the electromagnetic radiation.

light detection and ranging (LiDAR) – RS method that uses light in the form of a pulsed laser to measure ranges (variable distances) to the Earth, generating three-dimensional information about surface characteristics.

Landsat 8 (L8) - An EO satellite mission under the collaborative effort of the National Aeronautics and Space Administration (NASA) and the USGS from the United States. The mission was launched in February 2013.

near-infrared (NIR) - Light spectra with wavelengths within approximately 850-880 nanometers (nm).

normalized difference vegetation index (NDVI) – Quantifies vegetation by measuring the difference between NIR light wavelengths (which vegetation strongly reflects) and red light wavelengths (which vegetation absorbs).

North Carolina Geological Survey (NCGS) - The mission of the North Carolina Geological Survey is to provide unbiased and technically accurate applied earth science information to address societal needs (**NCGS, 2020**). Founded in 1823, the NCGS is the oldest Geological Survey in the United States (**Emmons, 1852**).

Observing Systems Capability Analysis and Review (OSCAR) - Quantitative user-defined satellite requirements for observation of physical variables in application areas under the WMO's mandate. OSCAR also provides detailed information on all earth observation satellites and instruments (**WMO, 2020**).

Operational Land Imager (OLI) - One of two remote sensing instruments on-board Landsat 8. The instrument can detect light wavelength including the visible range through the near-infrared in seven different spectral bands, in addition to a panchromatic band.

picture element (pixel) - The minimum discrete area of illumination on a digital display monitor.

principal component (PC) – A normalized linear combination of original variables which captures the maximum variance in a dataset; or left in a data set if higher order PCs have been accounted for.

principal component analysis (PCA) – A technique used to emphasize variation and bring out strong patterns in a dataset, via baseline coordinate transformations.

red-green-blue (RGB) - an additive color model in which red, green, and blue light are added together in various ways to reproduce a broad array of colors.

remote sensing (RS) - The process of detecting and monitoring the physical characteristics of an area, or object, by measuring its reflected and emitted radiation at a distance.

Sentinel-2 (S2) - An EO satellite mission designed and operated by the ESA. The mission is a constellation comprised of two twin satellites (2A and 2B) separated by 180 degrees on the same orbital path. The satellites were launched in June 2015 (2A) and in March 2017 (2B).

shortwave infrared (SWIR) - The light spectra range consisting of the wavelengths on the short end of the infrared designation.

synthetic aperture radar (SAR) – RS active sensor system that takes advantage of the long-range propagation characteristics of radar signals and the information processing capability of digital electronics to provide high-resolution imagery.

Thermal Infrared Sensor (TIRS) - One of two remote sensing instruments on-board Landsat 8. The instrument detects light wavelength in the thermal infrared range.

top-of-atmosphere (TOA) - The process of detecting and monitoring the physical characteristics of an area, or object, by measuring its reflected and emitted radiation at a distance.

United States Geological Survey (USGS) - Established by an act of Congress on March 3, 1879, to provide a permanent Federal agency to conduct the systematic and scientific

"classification of the public lands, and examination of the geological structure, mineral resources, and products of the national domain" (**USGS, 2020**).

visible/near infrared (VNIR) - A general designation comprising all the light spectra ranging from the visible wavelengths through the near-infrared wavelengths.

World Meteorological Organization (WMO) - A specialized agency of the United Nations, with a mandate to international cooperation and coordination on the state and behavior of the Earth's atmosphere, its interaction with the land and oceans, the weather and climate it produces, and the resulting distribution of water resources (**WMO, 2020**).

I. INTRODUCTION

Data collected by sensors on-board **Earth observation (EO)** satellites has revolutionized our knowledge of Earth's geology. The growing concern about where our future natural resources will come from and the natural hazards which we face has spurred great interest in finding new ways to evaluate the main variables of Earth's material and processes. Satellite **remote sensing (RS)** is a particularly valuable tool to collect critical information about the Earth's surface. The impacts of Earth's natural dynamics, in particular, require an up-to-date, spatially comprehensive, and large-scale source for geographical and geological data. Satellite EO provides broad, recurrent, and comprehensive views of the many dynamic processes that are affecting the resources and habitability of our planet.

This primer is an effort to acquaint those unfamiliar with spectral imagery from satellites with the basics of the technology, as it stands today. Further, it is also the ambition of the **North Carolina Geological Survey (NCGS)** that the reader will understand the value of satellite RS in geological investigations within our state. It is encouraged for the new-comer to satellite RS to refer to this document when exploring future geological research documents from the NCGS which uses this technology as a research tool. If the mineral exploration geologist or the engineering geologist looking for new investigation methods is inspired to use this technology for their own investigations in North Carolina, it's that much better for our State.

Scope – (1) Important to any satellite imagery scene investigation is an understanding of the sensors capturing the data and the various resolution considerations that are involved. After a discussion of the sensor resolution considerations, a summary of pre-processing corrections, Earth observation satellite orbits, and two of the most important satellite missions will all be considered. (2) Geological application for satellite imagery depends on the unique uses of several resolution factors, which will be highlighted. (3) After an image scene is captured, it is then visually analyzed and manipulated to accentuate features of the study focus. (4) Lastly, there is a discussion of light wavelength (spectra) band combinations, featuring those that have been proven useful for geological investigations.

II. SATELLITE IMAGERY

Satellite imagery, as a form of RS, provides a means to study objects of interest through sensors that do not have physical contact with it. EO from satellite imagery requires some kind of energy interaction between the target and the sensor. The sensor-detected signal may be solar energy that is reflected from the Earth's surface or it may be self-emitted energy from the surface itself. In addition to passive receivers, which can only detect energy when the naturally occurring energy is available, active sensors produce their own energy pulses and therefore are able to observe the Earth's surface regardless of solar conditions (**figure 1**).

Although satellite imagery is able to reveal information in the visible color spectrum (approximately 400 to 700 nanometers [nm]), the strength of its usefulness lies in its ability to capture data over various portions of the electromagnetic spectrum outside the visible range (**Elachi, 2006**) (**figure 2**). The visual representation of data outside the visible spectrum is achieved by assigning colors to the quantitative data to be viewed on a monitor.

A. Sensors

In the early days of EO, technologies were designed for general purpose platforms, which provide information for a wide range of applications. As the prices of both sensor and satellite platforms are rapidly decreasing, it is increasingly more common to design missions for specific variables. Therefore, they optimize for: (1) spatial, (2) temporal, and (3) spectral resolutions required for that target variable (**Elachi, 2006**). Radiometric resolution and angular resolution are additional resolution parameters relative to satellite imagery.

A scanning system used to collect data over a variety of different wavelength ranges is called a multispectral scanner (**Sabins, 1997**). There are two main modes or methods of scanning employed to acquire multispectral image data: (1) cross-track scanning and (2) along-track scanning (often referred to as "whisk-broom" and "push-broom" scanners, respectively) (**figure 3**). Cross-track scanners employ a faceted mirror that is rotated by a motor with a horizontal axis of rotation aligned parallel with the flight direction. The mirror sweeps across the terrain in a pattern of parallel scan lines oriented normal to the flight direction. Energy radiated or reflected from the ground is focused onto the detector by a secondary mirror. The **electromagnetic radiation (EMR)** is then split into its various wavelengths and focused onto additional detectors. The detectors measure ERM from a point on the ground, storing the value as a **digital number (DN)**, which is the radiometric intensity based on the radiometric resolution. Finally, the image is built of multiple rows of discrete ground segments called **picture elements (pixels)** (**Sabins, 1997**). Contrastingly, instead of a scanning mirror, along-track scanners use a linear array of detectors located at the focal plane of the image formed by a lens system and "pushed" along in the flight track direction. Each detector in the array is aimed at a specific point on the ground with the neighboring detector viewing the neighboring section of earth. The entire line of image data (line of pixels) is acquired at one time (**Sabins, 1997**). Along-track scanners are generally considered more advantageous for a number of reasons, namely: (1) they measure the energy from each ground resolution cell for a longer period of time (dwell time), (2) more energy is detected so more energy is available to improve the radiometric resolution, and (3) there are narrower bandwidths for each detector, which increases the spectral resolution (**USGS, 2012**).

1. Spatial Resolution (area)

Spatial resolution identifies the smallest object that can be detected on an image. Since images are mostly acquired in digital form, the spatial resolution is commonly expressed as the length (in meters) of the minimum spatial units in the image (pixels). Spatial resolution plays a major role in image interpretation because it affects the level of detail achieved. The interpreter can only identify objects several times larger than the pixel size (**Townshend, 1980**; **Sabins, 1997**) (**figure 4**), although smaller features can be detected when enough radiometric contrast between the object and the background exists.

2. Spectral Resolution (light wavelength)

Spectral resolution refers to the number of bands provided by the sensor and their spectral bandwidths (**figure 5a**). Generally speaking, a sensor will provide better discrimination capacity as more bands are acquired. Photographic systems acquire either panchromatic (one band) or color pictures (three bands). Digital sensors are generally multispectral (acquiring greater than three bands). The selection of the number of bands, width, and spectral range measured by the sensor is related to the objectives that it is expected to achieve (**Sabins, 1997**). While mining applications, for instance, require a fairly even usage of multiple bands in the visible, near-infrared, and mid-infrared ranges, a meteorological sensor usually requires an emphasis on the mid-infrared bands (**Van der Meer et al., 2017**).

3. Radiometric Resolution (light energy intensity)

Radiometric resolution denotes the sensitivity of the sensor. That is, its capacity to discriminate small variations in the recorded spectral radiance (**figure 5b**). In electronic sensors, the image is acquired digitally, and the radiometric resolution is commonly expressed as the range of values used for code in the input radiance or, more precisely, as the number of bits used to store the input signal (**Van der Meer et al, 2017**; **Sabins, 1997**). An 8-bit sensor system may discriminate 256 different input radiances per pixel (since each bit is binary, $2^8 = 256$, therefore a range of 0-255). Radiometric resolution is more critical in digital analysis than in visual analysis because the number of gray levels that the human eye is able to discern does not typically exceed 64 shades (**Sabins, 2017**). It may seem redundant to have even 256 digital values per band but, when the interpretation is digital, computers take advantage of all the available range, in which case high radiometric resolution is important to discriminate objects with similar spectral signatures.

4. Temporal Resolution (satellite recurrence time)

Temporal resolution refers to the observation frequency (revisiting period) provided by the sensor. Since the cycle is a function of the orbital characteristics of the satellite (height, speed, and declination), sensors with a high temporal resolution have coarse spatial resolution (**Sabins, 1997**), but will be able to observe a larger area in each image acquisition. The temporal resolution of an EO sensor system varies according to the objectives set for the mission. Satellites in geostationary orbit have temporal resolution independent of a satellite cycle because, by definition, the satellite is always in the target **field-of-view (FOV)**. Since satellites in geostationary orbit are fixed at a much higher altitude than satellites in polar (or near-polar) orbit they have an expansive FOV and therefore, a general rule-of-thumb suggests that the greater the temporal resolution is the worse the spatial resolution will be. Currently, for EO satellites in polar orbit, and fixed to a much lower altitude (the satellites of interest for geological and other Earth surface observations), temporal resolution varies from 16 days to 28 days (**Ose et al., 2016**). Obviously, with advancing technology and larger mission constellations, the temporal resolution will increase.

5. Angular Resolution (sensor position to FOV)

Angular resolution refers to the sensor's capacity to make observations of the same area from different viewing angles. As a basic concept, it is commonly assumed that terrestrial surfaces exhibit similar reflectance, independently of the observation angle. This may lead to notable errors, especially in those surfaces with strong directional effects when observed from different angles (**Diner et al., 1999**).

B. Image Pre-Processing Corrections

Geometric corrections – concerning errors introduced into the position of the imagery - are mostly corrected before the imagery is delivered to the end-user, fortunately. However, radiometric corrections, especially those related to the **top-of-atmosphere (TOA)** and to the Sun's angle, sometimes need to be massaged by the end-user analyst. All algorithms used to radiometrically correct imagery for Sun angle are based on computing the proportion of electromagnetic energy striking that particular place on the ground as defined by the cosine of the incidence angle (**Lu et al., 2008**; **Chuvieco, 2016**). In other words, knowing where the sun is and the slope of the terrain, the proportion of light recorded at that area on the ground can be determined. The relevant information needed can be found on the metadata text document that is downloaded with the scene imagery, namely: Sun's angle at the date and time of the imagery capture, the spectral bands additive scaling factor, and the spectral band reflectance multipliers.

The algorithm offered by the **United States Geological Survey (USGS)** is summed (**USGS, 2019**):

*TOA reflectance = [(spectral band reflectance multiplier) * (pixel value)] + radiance additive scaling factor*;

then, *correction for Sun's angle = TOA reflectance ÷ sin (Sun's elevation angle)*

C. EO Satellite Orbits

A first-order differentiation of EO satellites is based on modes of orbit. EO satellites are either geostationary or near polar orbiting. The former are located at very high equatorial orbits (approximately 36,000 km [22,370 mi]) (**USGS, 2019**; **ESA, 2015**) and always observe the same area. These geostationary satellites have a wide FOV to register the whole visible hemisphere of the planet in a single image. A network of geostationary satellites from different longitudes ensures coverage of the whole Earth. Geostationary satellites provide the best temporal resolution possible but at coarse spatial resolutions caused by the very high orbit. Weather monitoring satellites are the dominate satellites of this form.

Lower altitude sensors (typically between 700 and 900 km [435 to 560 mi]) comprise the near polar orbiting satellites (**USGS, 2019**; **ESA, 2015**) that are the focus of most non-weather related EO. Since the orbital plane is close to perpendicular to the equatorial plane, as the Earth rotates these satellites can observe different areas and cover a whole view of the planet in a certain number of hours or days, depending on the height and the sensor FOV (**figure 6**). A particular polar orbit of interest is "Sun-synchronous", where it is possible to acquire images at the same solar time, therefore facilitating multitemporal comparisons. There are some satellites in near-equatorial orbits, which are more suited to improve temporal resolution in tropical regions.

D. Satellite Missions – Landsat 8 and Sentinel-2 Comparison

The **World Meteorological Organization (WMO)** keeps an inventory of the world's EO satellite systems through its **Observing Systems Capability Analysis and Review** tool **(OSCAR)**. As of spring 2020, WMO counts 767 EO satellite missions - dating back to the earliest, NASA's Explorer-VII in October 1959 (**WMO, 2020**). When the decommissioned missions are filtered out, there are 239 that are clearly currently in operation. These missions are comprised of an overlapping collection of commercial satellites, very high altitude geostationary (inclined to weather monitoring) satellites, and satellites designed to capture data for very specific regions of Earth. The USGS superintends a repository for freely available (since 2008) moderate spectral resolution imagery from the United States' Landsat missions (**EarthExplorer, 2020**): the currently in-operation Landsat missions 7 and 8, as well as archival scenes, including

scenes from retired missions (Landsat 1-5). (Note that Landsat 6 failed at launch, while Landsat 9 is scheduled to launch and be operational by 2022.) Additionally, the USGS EarthExplorer site hosts the **European Space Agency's (ESA) Sentinel-2 (S2)** imagery for USGS clients, also free of charge.

As noted, there are numerous EO missions but when comparing for ease of access, quality of product, fees, and reliability, the Landsat and Sentinel missions are currently obvious choices to begin geological investigation from EO satellite missions. The **Landsat 8 (L8)** mission - launched in 2013- carries a two-sensor payload: **Operational Land Imager (OLI)** and the **Thermal Infrared Sensor (TIRS)** (**USGS, 2019**). The two instruments, OLI and TIRS, collect image data for nine shortwave bands (panchromatic band, inclusive) and two longwave thermal bands, respectively (**table 1**). The S2 mission -launched in 2015- is a constellation of two identical satellites phased 180 degrees from each other on the same orbit (**ESA, 2015**). S2 satellites each carry a single multi-spectral instrument (MSI) with 13 spectral channels in the **visible/near-infrared (VNIR)** and **shortwave infrared (SWIR)** spectral range, in addition to the dedicated aerosol detecting wavelengths band (**table 2**).

Both L8 and S2 are considered moderate spatial resolution (5 to 30 m^2) and high spectral resolution (8 to 49 bands); these parameter definitions are not formalized but are found commonly throughout the literature. As can be noted in tables 1 and 2, the spatial resolution for S2 is generally slightly better and S2 has more shortwave bands. L8 and S2 both have a radiometric resolution of 12-bits (potential DN range of 0-4095). L8 has a temporal resolution of 16 days but, partially because S2 is a constellation of 2 satellites, it has achieved a temporal resolution of 2-5 days. L8 contains a panchromatic band, making pansharpening to an effective higher resolution for mosaic images possible; S2 does not have a panchromatic band. Additionally, L8 hosts the TIRS sensor making thermal infrared differentiation possible, which is not an option for S2. Both systems are in a sun-synchronous orbit, allowing greater ease of temporal comparisons for scenes without as much correction post-processing needed.

III. GEOLOGICAL APPLICATIONS FOR SATELLITE IMAGERY

RS techniques generally have played a key role in geologic exploration because it is the most practical method of measuring many pertinent physical properties of large, inaccessible areas. The information derived provides a means for studying regional features, for extrapolating local measurements to regional scales, and for identifying critical areas for subsequent detailed studies. Ideally, an analysis should begin with large regions and then progress to successively smaller key areas. Such a multilevel approach has become one of the basic concepts of RS (**Colwell, 1983**). This sequence of study, it should be noted, is essentially the reverse of traditional geologic investigation, where detailed information is gathered for many small areas before regional features are delineated.

A. Unique Uses of Spatial Information (area)

Images displaying progressively larger areas show that different scales and types of information are revealed by changing the perspective. For example, major crustal breaks or faults are rarely exposed continuously for great distances. In fact, major faults are usually zones of smaller faults and related deformational features rather than a continuous single fracture. Satellite imagery is especially useful for regional landform studies because effective mosaics showing large areas at nearly uniform illumination can be compiled from these essentially planimetric images. One of the many important observations made from examination of these images and image mosaics are large linear features, which often do not appear on geologic maps composed using only traditional methods (**Rowan, 1975**). The use of these features has had a significant impact on regional geologic interpretations, including: mineral, petroleum, ground-water exploration, and earthquake studies.

B. Unique Uses of Spectral Information (light wavelength)

One of the main objectives of most geologic RS studies is to discriminate among different materials and ultimately to identify them, thereby aiding the mapping process fundamental to many geological investigations. In the visible part of the electromagnetic spectrum, some geologic materials are reasonably distinctive owing to brightness, color, or textural differences and can therefore be mapped on conventional black-and-white or color photographs (**Hunt, 1977**). Discrimination among many rock and soil units, however, can be improved substantially by also measuring radiation reflected in the NIR region. The spectral reflectance of rocks and soils is determined mainly by the oxidation-reduction state and coordination of the constituent transitional metal ions, commonly iron (**Pour et al., 2019**). Electronic transitions in these metal ions cause broad absorption bands which, although commonly conspicuous in spectra for individual iron-bearing minerals, are generally subdued in rock spectra where ferrous and nonferrous minerals are combined (**Van der Meer et al., 2017**; **Pour et al., 2019**). While the spectral reflectance differences between a few rock types are great enough to be detected by visually comparing the multispectral images, the differences among most rocks are so small that some form of image enhancement is needed to distinguish between them (**Hellman and Duncan, 2018**). Enhancement methods for spectral contrast employ, broadly, either a form of digital processing and/or color compositing. With digital processing, each of the pixels which constitute an individual multispectral band is divided by the spatially registered elements of another band (**Crippen and Blom, 2001**). The contrast of a selected part of the ratio values is enhanced, and the resulting values are used to record new black-and-white ratio images. The gray tones in these images show spectral radiance differences; variations due to albedo differences and topography are minimized. Color composites can also be prepared by assigning

a **red-green-blue (RGB)** color scheme to three ratios in use (**Cardoso-Fernandes et al., 2019**). Color from a viewing monitor (computer monitor, television screen, etc.) results from a different process than that due to reflection or transmission by a solid or solution; a monitor generates the three primary colors of light (red, green, and blue) and the different colors we see are due to different combinations and intensities of these three primary colors (**Elachi, 2006**).

C. Unique Uses of Temporal Information

Many geologic phenomena are manifestations of dynamic processes. Some, such as volcanic and earthquake activity or landslide hazards studies, such as those conducted by the landslide hazards group in the Asheville regional office of the NCGS (**Scheip and Wegmann, 2020**), are relatively short-lived catastrophic events, while others, including erosion and deposition, movement of crustal plates, and periodic seasonal and annual thermal variations, operate continuously over a longer period of time. Still other features are not dynamic in themselves, but their detection takes place over time. For example, the appearance of many landforms, especially linear structures, is influenced by seasonal variations in vegetation, soil moisture, and snow cover as well as by the shorter-term effects of illumination and atmospheric conditions (**Cudahy et al., 2016**). Owing to these factors, information gathered over time is essential for many remote-sensing geologic studies, although the time span may range from minutes or hours to several years. While aircraft can be used for monitoring predictable periodic variations of small areas, satellites are the most practical means of collecting information over time for large areas and for phenomena that are unpredictable or operate over longer periods.

IV. IMAGERY ANALYZED

A. Pansharpening

It is often desired to have the high spatial resolution and the high spectral resolution information combined in the same image file. Pansharpening is a type of data fusion that refers to the process of combining the lower resolution pixels (i.e., bands 1-7 in a L8 scene) with the higher resolution panchromatic pixels (i.e., band 8 in a L8 scene) to produce a high spatial resolution image. Many pansharpening techniques exist but, concisely, the algorithm is the conversion from RGB color space to hue intensity saturation color space. In hue intensity color space, the intensity component (I) is a simple average of the three color components represented by their radiometric intensity (their DN):

$$I = 1/3\ (R + G + B)$$

Most post-processing software applications use more robust versions of this simplified algorithm. For instance, **Environmental Systems Research Institute (ESRI)** allows for the

Brovey, Gram-Schmidt, intensity-hue-saturation, and simple mean transformations, as well as ESRI's own algorithm. Pansharpening serves the purpose of increasing the spatial resolution of an image in order to identify objects based on shape and texture. However, with increased spatial resolution, there is a distortive cost to the spectral resolution (**figure 7**). Pansharpening is not advised if the immediate analysis objective is spectral in nature.

1. Brovey Transformation

The Brovey transformation is based on spectral modeling and was developed to increase the visual contrast in the high and low ends of the data's histogram. It is a method that multiplies each resampled, multispectral pixel by the ratio of the corresponding panchromatic pixel intensity to the sum of all the multispectral intensities. It assumes that the spectral range spanned by the panchromatic image is the same as that covered by the multispectral channels (**Mandhare et al., 2013**). The general equation uses the RGB and the panchromatic bands as inputs to output new RGB bands. For example:

$$R\ (out) = R\ (in) \div [(B\ (in) + G\ (in) + R(in)) * (panchromatic)]$$

2. Gram-Schmidt Transformation

The Gram-Schmidt transformation takes in vectors that are not orthogonal, and then rotates them so that they are orthogonal afterward. In the case of images, each band (panchromatic, R, G, B, infrared) corresponds to on high-dimensional vector (**Mhangara et al., 2020**; **Grochala and Kedzierski, 2017**). The first step creates a low-resolution pan band by computing a weighted average of the multispectral bands. Next, these bands are decorrelated using the Gram-Schmidt orthogonalization algorithm, treating each band as one multidimensional vector. The simulated low-resolution panchromatic band is used as the first vector; which is not rotated or transformed. The low-resolution panchromatic band is then replaced by the high-resolution panchromatic band, and all bands are back-transformed in the higher resolution.

3. Intensity-Hue-Saturation Transformation

The IHS method converts the multispectral image from RGB to intensity, hue, and saturation. The low-resolution intensity is replaced with the high-resolution panchromatic image. Then, the image is back-transformed from IHS to RGB in the higher resolution (**Ling et al., 2007**).

4. Simple Mean Transformation

The simple mean transformation method applies a simple mean averaging equation to each of the output band combinations.

B. Image Stretch

Displaying images at optimal contrast allows the analyst to resolve features of interest that might not otherwise be visible or perceptible. Often, the range of values that an image contains is not correctly stretched across the range the computer can display and, as a result, the image may appear dark or have little contrast. Applying a contrast stretch takes full advantage of the range of values the computer can display by stretching the range of values in the image to the full range of values available to the computer display. There are usually several different types of stretch options with most image processing software packages (**Chib and Devi, 2016**). For instance, ESRI offers the ability to use a minimum-maximum stretch that uses the entire range of image values and stretches them across the full radiometric resolution range of grayscale values allowable, given the radiometric resolution. If, for instance, an image has a value range from 110 to 2030 and a minimum-maximum stretch is applied to an image pixel with a value of 110, it will become 0 (black) in the stretched image. An image pixel with a value of 2030 will become 4096 (white) in an image scene with 12-bit radiometric resolution ($2^{12} = 4096$). Everything between 110 and 2030 in the image will stretch accordingly, linearly. Standard deviation is another common stretch method. A standard deviation stretch sets the pixels with very low and very high pixel values, in a 12-bit image, to 0 and 4096 respectively, stretching the pixel values in between. In this case, pixel values falling outside a specified standard deviation value will be all black (low end) or all white (high end), while the pixel values in between are distributed normally (**Chuvieco, 2016**). Standard deviation is most successful when there are outliers at the radiometric extremes, with the majority of the rest of the image pixels falling closer to the radiometric median (**figure 8**).

C. Filtering

Image filters can sometimes highlight features of interest that are not human-perceptible in the unenhanced version of the image. Image filters work by assigning a new value to each pixel in an image based on that pixel's value and the values of neighboring pixels (**Schowengerdt, 2007**). In addition to setting the shape and dimensions of the neighborhood and the function that is assigned to the processing cell, most image filtering algorithms provide the ability to configure the weights that each neighbor has in the function being applied to the neighborhood as the "moving window" shifts across the image.

1. Low-Pass Filters (Smoothing)

Low-pass filters are useful for removing anomalous ("noisy") pixels from an image and creating smoother, often more visually appealing images. If a pixel is slightly different from its neighbors in an image, a low-pass filter will decrease this difference and make the pixel in the output image appear more similar to it neighbors. In doing so, a low-pass filter reduces local variation and extreme values in an image. Low-pass filters typically apply a mean function to the neighborhood with the mean value applied to the focus pixel (**Cushnie and Atkinson, 1985**). Seeing that a smoothing effect through a neighborhood of pixels is then hopefully easier to understand when a mean weight value is applied (**figure 9**). Low-pass filtering has not been used frequently in geological investigations. It would be most effective when trying to follow spatially extensive general trends.

2. High-Pass Filters (Edge Location)

High-pass filters are useful for identifying edges in an image or sharpening an image. These types of filters enhance fine-scale, local details in an image and accentuate edges. If a pixel is slightly different from its neighbors, a high-pass filter will accentuate this difference in the output by adding contrast (**de Jong, 1993**). High-pass filters also use the concept of the neighborhood and the moving window, previously discussed. Typically, high-pass filters use a multiplier as their function, sometimes with weights applied to the neighborhood pixels (figure 9). Geologists get the added benefit from using multispectral images because shortwave infrared bands are sensitive to changes in soil and rock content, making it possible to differentiate some basic rock types. Directional filters are a specialized high-pass filter which can take advantage of the angle of reflectance created a subtle change in the ground surface angle to the Sun, or by a change of a dominate mineral (indicating a possible change in lithology) with a different crystal face angle to the Sun.

V. SPECTRAL BANDS

Earth's atmosphere is not well-suited for transmitting light because gases and aerosols absorb and scatter the light; the same effect happens to images captured from space. Fortunately for EO analysts light has an advantageous property: longer wavelengths are less affected by absorption and scattering. In addition to the red, green, and blue spectral wavelength bands, satellite sensors also capture wavelengths in the near-infrared and shortwave infrared bands – well beyond the visible spectrum. L8 and S2 also capture ultra-blue wavelengths (although not normally much use for mineral/geological studies). Again, images that include both visible and non-visible bands are multispectral images.

Computer displays only have red, green, and blue pixels and they can only display the visible spectrum wavelengths. To navigate this issue, the analyst will assign bands from a multispectral image to the red, green, and blue pixels of the computer display, producing a false-color image. For instance, an infrared band might be assigned to the red pixels, the NIR band to the green pixels, and the visible-red band to the blue pixels. A natural-color image would then be an assignment of the visible-red band to the red pixels, visible-green to the green pixels, and the visible-blue to the blue pixels. Conventionally, wavelength band assignment works in the direction of increasing wavelength order; the shortest wavelength band is usually assigned to blue pixels, the next longest wavelength band to green pixels, and the longest wavelength band to red pixels. There are occasional exceptions.

A. Common Band Assignments for Geology

An obvious starting approach for a geological analyst is to use proven wavelength band assignments. For preliminary geological investigation, it is important to appreciate the basis for inter-band contrast enhancement. Band combinations with the lowest inter-band correlation usually are found between a band from the SWIR, the NIR, and one of the visible bands. Combinations using this general scheme will usually provide the most detail without additional enhancement. An analyst will readily notice that the same band combinations often reveal different features in arid verses highly vegetated environs. It is essential that the analyst has a reasonable ground-truth information before starting. Listed below are some of these common band assignments, as R-B-G, for L8, with the S2 equivalents (also, refer to tables 1 and 2 for band number assignments relative to light wavelengths).

1. L8: 4-3-2 (S2: 4-3-2)

This is the assignment approximating natural color (**figure 10**, top-left).

2. L8: 5-4-3 (S2: 5-4-3)

This assignment reproduces a traditional infrared aerial photograph. Vegetation will display red, water as black, and rock and soil as shades of gray or brown. This assignment highlights the boundaries between vegetated and barren land but cannot differentiate agricultural plots very well (**figure 10**, bottom-left).

3. L8: 7-5-2 (S2: 12-8A-2)

This assignment often produces rocky outcrops (both mafic and felsic dominated) in shades of red, purple, and blue. Many structural features might be visible if there is sparse vegetation. Variations in regolith geology often appear as a patchwork of yellows, browns, and light greens. Agricultural plots are usually more distinguishable. L8: 7-5-3, 6-5-2, and 6-5-3 (S2: 12-8A-3, 11-8A-2, and 11-8A-3) are sometimes close substitutes for this overall affect (**figure 10**, bottom right).

B. Derivative Bands

In addition to the original bands of imagery that are recorded by a sensor, it is possible to calculate a number of additional bands from the original bands. Derivative bands include simple ratios, transformations, or indices that are created to reveal or enhance the link between the variation in the image and the variation on the ground surface. Some of these derivative bands have been developed from theoretical knowledge of the physical and chemical properties of the material being sensed while others have been empirically derived from observation. In either case, the goal is to tease more information from the imagery as it relates to what is happening in real space.

C. Ratios and Indices

1. Ratios

As its name implies, is created simply when one original band is divided by another to create a new derivative band. Band ratios highlight the spectral differences that are unique to the materials of interest by creating additional contrast. Identical surface materials can give different brightness values because of the topographic slope and aspect, shadows (particularly from clouds), or seasonal changes in sunlight illumination angle and intensity. There are several ratio combinations that have proven useful for geology investigations (**table 3**) (**figure 11**).

2. Indices

Indices are some form of a ratio of the original spectral bands, sometimes with other factors or coefficients included. By far, the most common index is the **Normalized Difference Vegetation Index (NDVI)** (**Anderson et al., 1976**) and is expressed as:

$$NDVI = (NIR\ band - red\ band) \div (NIR\ band + red\ band)$$

This particular index is useful to geological investigators for identifying pixel clusters that are not of analysis interest (vegetation surface cover). Note that if the geological investigation is geomorphological in nature then the change is vegetation over time (temporal resolution) is what is an integral component of the analysis. There is a plethora of indices that can be created; the utility of each will be situational to the study area and study purpose. This again emphasizes the need for the geological RS analyst to have a good understanding of what should be generally expected. Knowledge of the area-of-interest is crucial before starting an RS analysis.

D. Transformations - PCA

Transformations are more complex than ratios and will result in the same number of derivative bands as there were original spectral bands. However, the new derivative bands will be changed or transformed in some unique way. There are two common transformations used by EO analysts; the first is **Principal Components Analysis (PCA)**. The second is Tasseled-Cap Transformation which is not as common with geological investigations; however, its existence should be noted here.

PCA is performed from a statistical basis of data reduction by transforming the imagery into independent derivative bands in which the variance of the imagery is maximized into the first few principal components (**figure 12**). PCA transformation is used to remove the redundancy between the original bands and create independent orthogonal transformed bands (Estornel et al., 2013). Because the original image bands are so highly correlated, creating PCA bands has the advantage of creating new independent transformed bands and potentially reducing the number of bands needed. Band reduction occurs because when creating independent transformed bands, the majority of the variance in all the original spectral bands is now represented by the first **principal component (PC)**. Further, it is common for up to 95% of the original spectral bands image variance to be represented by the first three PCs (Estornel et al., 2013). By creating a PCA, the image analyst has another means (quantitative) for estimating image spectral band combinations (**figure 13**), which can then be used for a more complete visual estimation of potentially successful spectral band combinations (**figure 14**).

VI. CONCLUSION

Image scene capture by an Earth-orbiting satellite is fundamentally defined by the resolutions of the sensors' design parameters: spatial, spectral, radiometric, temporal, and angular. Spatial resolution describes how much detail in a photographic image is visible to the human eye. Spectral reflectance (or signatures) of different types of ground targets provide the knowledge base for information extraction and are recorded in "bands" by the sensors. Every time an image is acquired by a sensor, its sensitivity to the magnitude of the electromagnetic energy determines

the radiometric resolution; the finer the radiometric resolution of a sensor, the more sensitive it is to detecting small differences in reflected or emitted energy. The satellite visitation period over an area of interest is a crucial consideration when the concern is change over time, especially for sudden or punctuated events, such as landslides, flooding, and earthquakes. The angular resolution of the satellite to the FOV is an essential pre-processing consideration, if the image is "raw" (not calibrated or corrected before the scene data is distributed to the end-user). EO satellites are typically low-altitude and near-polar orbiting (often Sun-synchronous) when the scope is land observation rather than weather observation. The Landsat and Sentinel missions, under the management domain of the United States and the European Union, respectively, have been a powerful tool for remote sensing geology investigations as far back as the first Landsat mission launch in 1972.

When considering different image enhancement techniques by the analyst, it is usually important to experiment with as many methods as possible to achieve the highlight contrast that is being sought. If the analyst is interested in enhancing the spatial resolution with pansharpening, multiple transformation methods should be used to isolate the most-favored outcome. The same concept is true, if not more so, for contrast stretching methods. Filtering techniques are somewhat more dependent of what the desired affect is. If a smoothing effect for large area features is desired, then a low-pass filter method is where the analyst should begin. If the desired effect is edge detection, the analyst should try high-pass filter approaches.

A PCA can help eliminate a lot of fruitless trial-and-error by quantitatively showing most-favored band contrasts. Proven spectral band assignments, derivative bands, and ratios also have given the new analyst some breathing room when choosing a place to start after an image scene has been acquired.

Mapping minerals from space was one of the main motivating reasons for creating the earliest multispectral satellite systems when Landsat 1 was launched in 1972 (**Cudahy et al., 2016**). Since that period, improved resolutions have allowed for different techniques and new functions. Satellite RS is a rapidly changing technology and therefore an exciting time for geo-scientists interested in utilizing the tool. In the past, mapping potential mineral deposits using satellite imagery has been mostly relegated to arid, sparsely vegetated locations, such as the western United States and interior Australia (**Rockwell, 2013**; **Cudahy et al., 2016**); however, new techniques from researchers in Brazil and southeast Asia have opened the door to the mineral exploration potential of the more humid, vegetated climes of Earth (**Poppiel et al., 2020**; **Magiera, 2018**), including the southeast United States. Beyond mineral exploration, more traditional geology bedrock mapping ventures can also benefit from satellite imagery. Directional filters, for instance, have the potential to "pull out" lineament features, aiding in identifying and more accurately positioning surficially-expressed faulting (**Farahbakhsh et al., 2018**). With hyperspectral imagery, differentiating lithology within a sequence is also possible (**Kruse et al., 2003**; **Boesche et al., 2015**).

Combining satellite imagery with other forms of RS including aeromagnetic surveys, **synthetic aperture radar (SAR)**, and **light detection and ranging (LiDAR)** has the most immediate potential for new exploration and mapping uses. The NCGS already uses satellite RS extensively with the geologic hazards-landslides mapping group in the Asheville Regional Office (ARO; Swannanoa, North Carolina) (**Scheip and Wegmann, 2020**). We are currently attempting to use satellite imagery, as described here, to aid in locating potential placer mineral reserves for the benefit of North Carolina's citizens and economy. In the future, hopefully other uses, such as mapping faults and other lineament features, will be forthcoming. As always, any tool in the service of geological investigations is an aid, not a substitute, for in situ observations when possible.

REFERENCES CITED

[1]Where available, URL addresses are provided for on-line documents (current to publication date of this document).

[2]If a document is not available, via open-source, the document was obtained by making a copy request to the first-author, or arbiter, of the document.

[3]All books used as a resource were located in a university library.

[4]Some documents are offered in pre-print format as of the printing date of this document; it will therefore likely be possible to find a further edited final-print version in the future.

Anderson, J.R., Hardy, E.E., Roach, J.T., and Witmer, R.E., 1976, A Land Use and Land Cover Classification System for Use with Remote Sensor Data: U.S. Geological Survey Professional Paper 964, 27 p. URL: https://pubs.usgs.gov/pp/0964/report.pdf

Boesche, N., Rogass, C., Lubitz, C., Brell, M., Herrmann, S., Mielke, C., Tonn, S., Appelt, O., Altenberger, U., and Kaufmann, H., 2015, Hyperspectral REE (Rare Earth Element) Mapping of Outcrops - Applications for Neodymium Detection: Remote Sensing, v. 7, p. 5160-5186, DOI:10.3390/rs70505160. URL: https://www.researchgate.net/publication/275406875_Hyperspectral_REE_Rare_Earth_Element_Mapping_of_Outcrops-Applications_for_Neodymium_Detection#fullTextFileContent

Boussaa, S., Kheloufi, A., Zaourar, N., and Bouachma, S., 2017, Iron and Aluminum Removal from Algerian Silica Sand by Acid Leaching: Acta Physica Polonica Series A, v. 132, no. 3-II, DOI:10.12693/APhysPolA.132.1082. URL: https://www.researchgate.net/publication/320649513_Iron_and_Aluminium_Removal_from_Algerian_Silica_Sand_by_Acid_Leaching

Cardoso-Fernandes, J., Teodoro, A.C., and Lima, A., 2019, Remote sensing data in lithium (Li) exploration: A new approach for the detection of Li-bearing pegmatites: International Journal of Applied Earth Observation and Geoinformation, v. 76, p. 10-25, DOI:10.1016/j.jag.2018.11.001.

Chib, S., and Devi, S., 2016, Performance Analysis of Enhancement Techniques for Satellite Images: International Journal of Computer Sciences and Engineering, v. 4(12), E-ISSN: 2347-2693. URL: https://www.academia.edu/30829746/Performance_Analysis_of_Enhancement_Techniques_for_Satellite_Images

Chuvieco, E., 2016, Fundamentals of Satellite Remote Sensing: An Environmental Approach (second edition): Boca Raton, FL, CRC Press, 468 p.

Colwell, R.N., 1983, Manual of Remote Sensing (second edition): American Society of Photogrammetry, 2440 p.

Crippen, R.E., and Blom, R.G., 2001, Unveiling the Lithology of Vegetated Terrains in remotely Sensed Imagery: Photogrammetric Engineering and Remote Sensing, v. 67, no. 8, p. 935-943. URL: https://www.asprs.org/wp-content/uploads/pers/2001journal/august/2001_aug_935-943.pdf

Cudahy, T., Caccetta, M., Thomas, M., Hewson, R., Abrams, M., Kato, M., Kashimura, O., Ninomiya, Y., Yamaguchi, Y., Collings, S., Laukamp, C., Ong, C., Lau, I., Rodger, A., Chia, J., Warren, P., Woodcock, R., Fraser, R., Rankine, T., Vote, J., de Caritat, P., English, P., Meyer, D., Doescher, C., Fu, B., Shi, P., and Mitchell, R., 2016, Satellite-derived mineral mapping and monitoring of weathering, deposition and erosion: Scientific Reports, v. 6(23702), DOI:10.1038/srep23702. URL: https://www.nature.com/articles/srep23702

Cushnie, J., and Atkinson, P., 1985, The effect of spatial filtering on scene noise and boundary detail in Thematic Mapper imagery: Photogrammetric Engineering and Remote Sensing, 51(9), p. 1483-1493. URL: https://www.asprs.org/wp-content/uploads/pers/1985journal/sep/1985_sep_1483-1493.pdf

Diner, D., Asner, G., Davies, R., Knyazikhin, Y., Muller, J., Nolin, A., Pinty, B., Schaaf, C., and Stroeve, J., 1999, New directions in Earth observing: Scientific applications of multiangle remote sensing: Bulletin of the American Meteorological Society, v. 80(11), p. 2209-2228. URL: https://ir.library.oregonstate.edu/concern/parent/dv13zv88s/file_sets/wp988m347

Drury, S., 1987, Image Interpretation in Geology: London, Allen and Unwin, 243 p.

EarthExplorer, 2020, USGS remote sensing imagery database. URL: https://earthexplorer.usgs.gov/

Elachi, C., 2006, Introduction to the Physics and Techniques of Remote Sensing, 2nd Edition: New York, John Wiley & Sons, 552 p.

Emmons, E., 1852, Report of Professor Emmons, on His Geological Survey of North Carolina: S. Gales (printer to the legislature), 183 p. URL: https://archive.org/details/reportprofessor00geolgoog/mode/2up

ESA, 2015, Sentinel-2 User Handbook; ESA Standard Document, issue 1, rev. 2. URL: https://sentinel.esa.int/documents/247904/685211/Sentinel-2_User_Handbook

ESA, 2020, European Space Agency. URL: http://www.esa.int/

Estornell, J., Marti-Gavila, J., Sebastia, M., Mengual, J., 2013, Principal component analysis applied to remote sensing: MSEL, v. 6(2), no. 7, ISSN:19883145. URL: https://www.researchgate.net/publication/259638444_Principal_component_analysis_applied_to_remote_sensing

Farahbakhsh, E., Chandra, R., Olierook, H., Scalzo, R, Clark, C., Reddy, S., and Muller, R., 2018, Computer vision-based framework for extracting geological lineaments from optical remote sensing data (pre-print): arXiv:1810.02320v1. URL: https://arxiv.org/abs/1810.02320

Grochala, A. and Kedzierski, M., 2017, A method of panchromatic image modification for satellite imagery data fusion: Remote Sensing, v. 9(639), DOI:10.3390/rs9060639. URL: https://www.researchgate.net/publication/317819845_A_Method_of_Panchromatic_Image_Modification_for_Satellite_Imagery_Data_Fusion

Hellman, P., and Duncan, R., 2018, Evaluating Rare Earth Element Deposits: ASEG Extended Abstracts, 2018:1, p. 1-13, DOI:10.1071/ASEG2018abT4_3E. URL: https://www.researchgate.net/publication/323452073_Evaluating_Rare_Earth_Element_Deposits

Hunt, G., 1977, Spectral signatures of particulate minerals in the visible and near-infrared: Geophysics, v. 42(3), p. 501-513.

Jensen, J., 2016, Introductory Digital Image Processing: A Remote Sensing Perspective, 4th Edition: Pearson Publishing, 656 p.

de Jong, S., 1993, An application of spatial filtering techniques for land cover mapping using TM-images: Geocarto International, v. 1, p. 43-49, DOI:10.1080/10106049309354398.

Kruse, F., Boardman, J., and Huntington, J., 2003, Comparison of Airborne Hyperspectral Data and EO-1 Hyperion for Mineral Mapping: IEEE Transactions on Geoscience and Remote Sensing, v. 41, no. 6, DOI:10.1109/TGRS.2003.812908. URL: https://www.researchgate.net/publication/3203214_Comparison_of_Airborne_Hyperspectral_Data_and_EO-1_Hyperion_for_Mineral_Mapping

Lillesand, T., Kiefer, R., and Chipman, J., 2015, Remote Sensing and Image Interpretation, 7th Edition: John Wiley and Sons, 736 p.

Ling, Y., Ehlers, M., Usery, E., and Madden, M., 2007, FFT-enhanced HIS transform method for fusing high-resolution satellite images: ISPRS Journal of Photogrammetry & Remote Sensing, v. 61(6), p. 381-392, DOI:10.1016/j.jsprsjprs.2006.11.002. URL:

https://www.researchgate.net/publication/223909867_FFT-enhanced_IHS_transform_for_fusing_high-resolution_satellite_images

Lu, D., Ge, H., He, S., Xu, A., Zhou, G., and Du, H., 2008, Pixel-based Minnaert Correction Method for Reducing Topographic Effects on a Landsat 7 ETM+ Image: Photgrammetric Engineering and Remote Sensing, v. 74(11), p. 1343-1350, DOI:10.14358/PERS.74.11.1343. URL: https://www.researchgate.net/publication/235244169_Pixel-based_Minnaert_Correction_Method_for_Reducing_Topographic_Effects_on_a_Landsat_7_ETM_Image

Magiera, J., 2018, Can Satellite remote Sensing be Applied in Geological Mapping in Tropics?: E3S Web of Conferences, v. 35(02004), DOI:10.1051/e3sconf/20183502004. URL: https://www.e3s-conferences.org/articles/e3sconf/pdf/2018/10/e3sconf_polviet2018_02004.pdf

Mandhare, R.A., Upadhyay, P., and Gupta, S., 2013, Pixel-level image fusion using Brovey transform and wavelet transform: International Journal of Advanced Research in Electrical, Electronics and Instrumentation Engineering, v. 2(6), ISSN(Print):23203765, ISSN(Online):22788875. URL: https://www.ijareeie.com/upload/june/25F_PIXEL.pdf

Mhangara, P., Mapurisa, W., and Mudau, N., 2020, Comparison of Image Fusion Techniques Using Satellite Pour l'Observation de la Terre (SPOT) 6 Satellite Imagery: Applied Sciences, v. 10(5):1881, DOI:10.3390/app10051881. URL: https://www.researchgate.net/publication/339833053_Comparison_of_Image_Fusion_Techniques_Using_Satellite_Pour_l'Observation_de_la_Terre_SPOT_6_Satellite_Imagery

NCGS, 2020, NC Geological Survey: North Carolina Department of Environmental Quality. URL: https://deq.nc.gov/about/divisions/energy-mineral-land-resources/north-carolina-geological-survey

Ose, K., Corpetti, T., Demagistri, L., 2016, Multispectral Satellite Image Processing, *in* Baghdadi, N. and Zribi, M., eds., Optical Remote Sensing of Land Surface: Techniques and Methods, 1st Edition: France, Elsevier, 388 p.

Poppiel, R., Lacerda, M., Rizzo, R., Safanelli, J., Bonfatti, B., Silvero, N., and Dematte, J., 2020, Soil Color and Mineralogy Mapping Using Proximal and Remote Sensing in Midwest Brazil: Remote Sensing, 12(7), 1197, DOI:10.3390/rs12071197. URL: https://www.mdpi.com/2072-4292/12/7/1197/htm

Pour, A., Hashim, M., Hong, J., and Park, Y., 2019, Lithological and alteration mineral mapping in poorly exposed lithologies using Landsat 8 and ASTER satellite data: North-eastern Graham Land, Antarctic Peninsula: Ore Geology Reviews, v. 108, p. 112-133, DOI:10.1016/j.oregeorev.2017.07.018. URL:

https://www.researchgate.net/publication/318853912_Lithological_and_alteration_mineral_mapping_in_poorly_exposed_lithologies_using_Landsat-8_and_ASTER_satellite_data_North-eastern_Graham_Land_Antarctic_Peninsula

Rockwell, B., 2013, Automated Mapping of Mineral Groups and Green Vegetation from Landsat Thematic Mapper Imagery with an Example from the San Juan Mountains, Colorado: USGS Scientific Investigations Map 3252, 25 p. pamphlet, 1 map sheet, scale 1:325,000. URL: https://www.researchgate.net/publication/278017705_Automated_Mapping_of_Mineral_Groups_and_Green_Vegetation_from_Landsat_Thematic_Mapper_Imagery_with_an_Example_from_the_San_Juan_Mountains_Colorado#fullTextFileContent

Rowan, L., 1975, Iron-absorption band analysis for the discrimination of iron-rich zones: NASA Type-II report, 14 p. URL: https://pubs.usgs.gov/of/1973/0245/report.pdf

Sabins, Floyd F., 1997, Remote Sensing Principles and Interpretation, 3rd Edition: Long Grove, Illinois, Waveland Press, Inc., 449 p.

Scheip, C., and Wegmann, K., 2020, HazMapper: A global open-source natural hazard mapping application in Google Earth Engine: Natural Hazards and Earth System Sciences (pre-print), DOI:10.5194/nhess-2020-108. URL: https://www.researchgate.net/publication/341039360_HazMapper_A_global_open-source_natural_hazard_mapping_application_in_Google_Earth_Engine

Schowengerdt, R., 2007, Remote Sensing, Models, and Methods for Image Processing, 3rd Edition: Burlington, MA, Elsevier Academic Press, 560 p.

Segal, D., 1982, Theoretical Basis for Differentiation of Ferric-Iron Bearing Minerals, Using Landsat MSS Data: Proceedings of Symposium for Remote Sensing of Environment, 2nd Thematic Conference on Remote Sensing for Exploratory Geology, Fort Worth, TX, p. 949-951.

Sultan, M., Arvidson, R., Sturchio, N., Guinnes, E., 1987, Lithologic mapping in arid regions with Landsat TM data: Meatiq dome, Egypt: Geological Society of America Bulletin 99, p. 748-762. URL: https://www.researchgate.net/publication/249526042_Lithologic_mapping_in_arid_regions_with_Landsat_Thematic_Mapper_data_Meatiq_Dome_Egypt

Tipler, P., 1999, Physics for Scientists and Engineers: Vol. 1: Mechanics, Oscillations and Waves, Thermodynamics: MacMillian, 454 p.

Townshend, J., 1980, The Spatial Resolving Power of Earth Resources Satellites: A Review: Greenbelt, MD, NASA, Goddard Spaceflight Center, 36 p. URL: https://ntrs.nasa.gov/archive/nasa/casi.ntrs.nasa.gov/19810012912.pdf

USGS, 2012, Multispectral Scanner (MSS) Geometric Algorithm Description Document (ADD): LS-IAS-06, version 1.0, 110 p. URL: https://landsat.usgs.gov/sites/default/files/documents/LS-IAS-06.pdf

USGS, 2019, Landsat 8 (L8) Data Users Handbook: LSDS-1574, version 5.0, 106 p. URL: https://prd-wret.s3.us-west-2.amazonaws.com/assets/palladium/production/atoms/files/LSDS-1574_L8_Data_Users_Handbook-v5.0.pdf

USGS, 2020, United States Geological Survey mission statement. URL: https://govinfo.library.unt.edu/npr/library/status/mission/musgs.htm

Van der Meer, F.D, van der Werff, H.M.A., and van Ruitenbeck, F.J.A., 2017, Potential of ESA's S2 for geological applications: Elsevier, (pre-print).

Weem, R. and Lewis, W., 2007, Detailed Sections from Auger Holes in the Roanoke rapids 1:100,000 Map Sheet, North Carolina: USGS, OFR 2007-1092. URL: https://pubs.usgs.gov/of/2007/1092/

Weems, R., Lewis, W., and Aleman-Gonzalez, W., 2009, Surficial Geologic Map of the Roanoke Rapids 30' x 60' Quadrangle, North Carolina: USGS, OFR 2009-1149. URL: https://pubs.usgs.gov/of/2009/1149/

WMO, 2020, Observing Systems Capability Analysis and Review Tool (OSCAR) database. URL: https://oscar.wmo.int/surface/#/

ACKNOWLEDGEMENT

This primer was improved by comments and suggestions from NCGS colleagues, Dr. Kenneth B. Taylor and Dwain M. Veach.

FIGURES

All figures created by J. Chapman, unless otherwise noted.

Figure 1. Passive vs. Active Satellite Sensors.

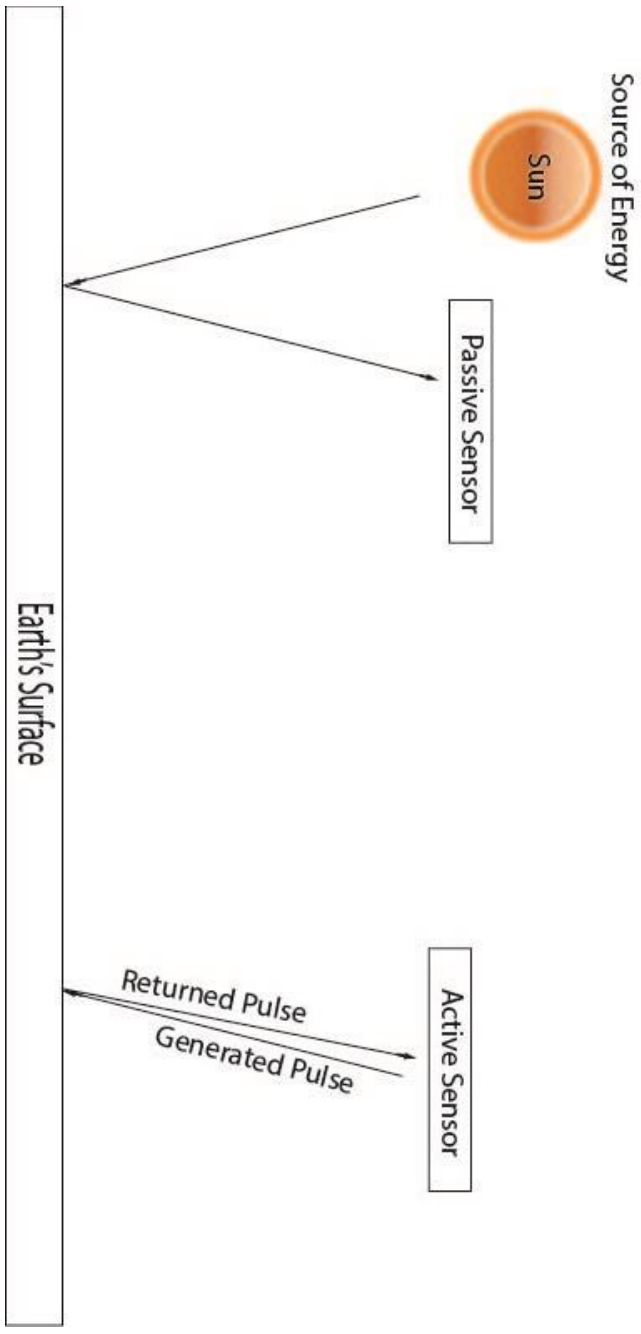

Figure 2. Visible Portion of the Light Wavelength Spectrum. Ultraviolet (UV) wavelengths are shorter than the visible spectrum so they are off the chart, below approximately 400 nm. Near-Infrared (NIR) wavelengths are longer than the visible spectrum so they are off the chart above approximately 700 nm.

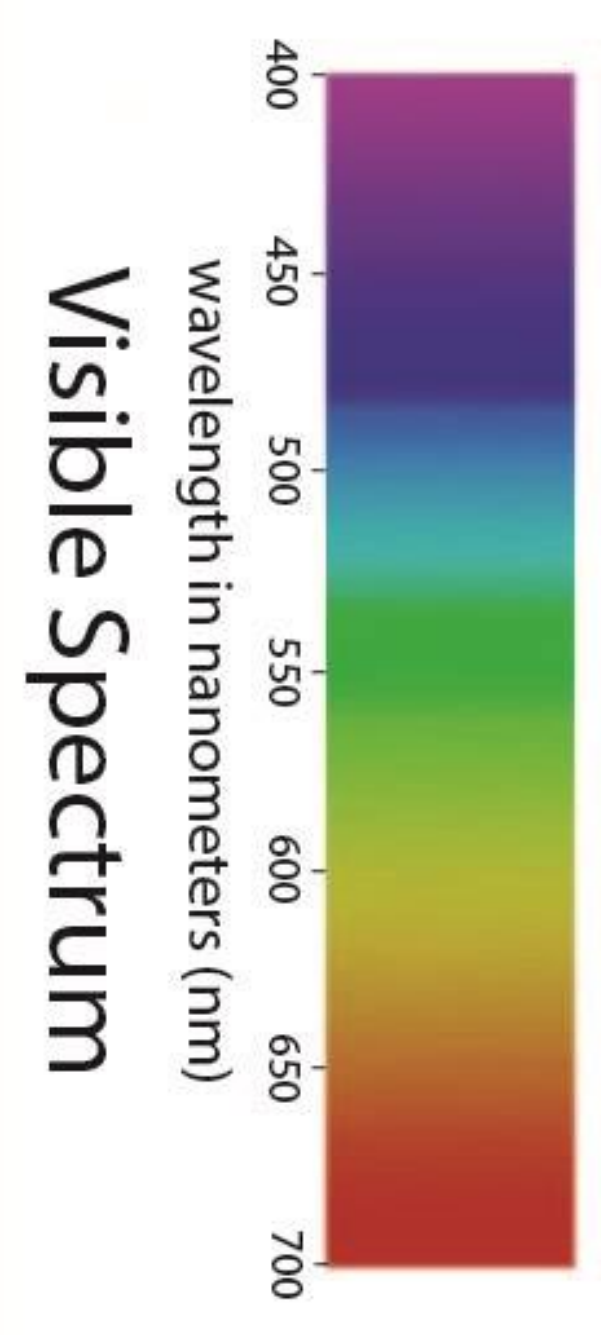

Figure 3. Cross-Track "whisk-broom" Scanner (left) vs. Along-Track "push-broom" (right) Scanner.

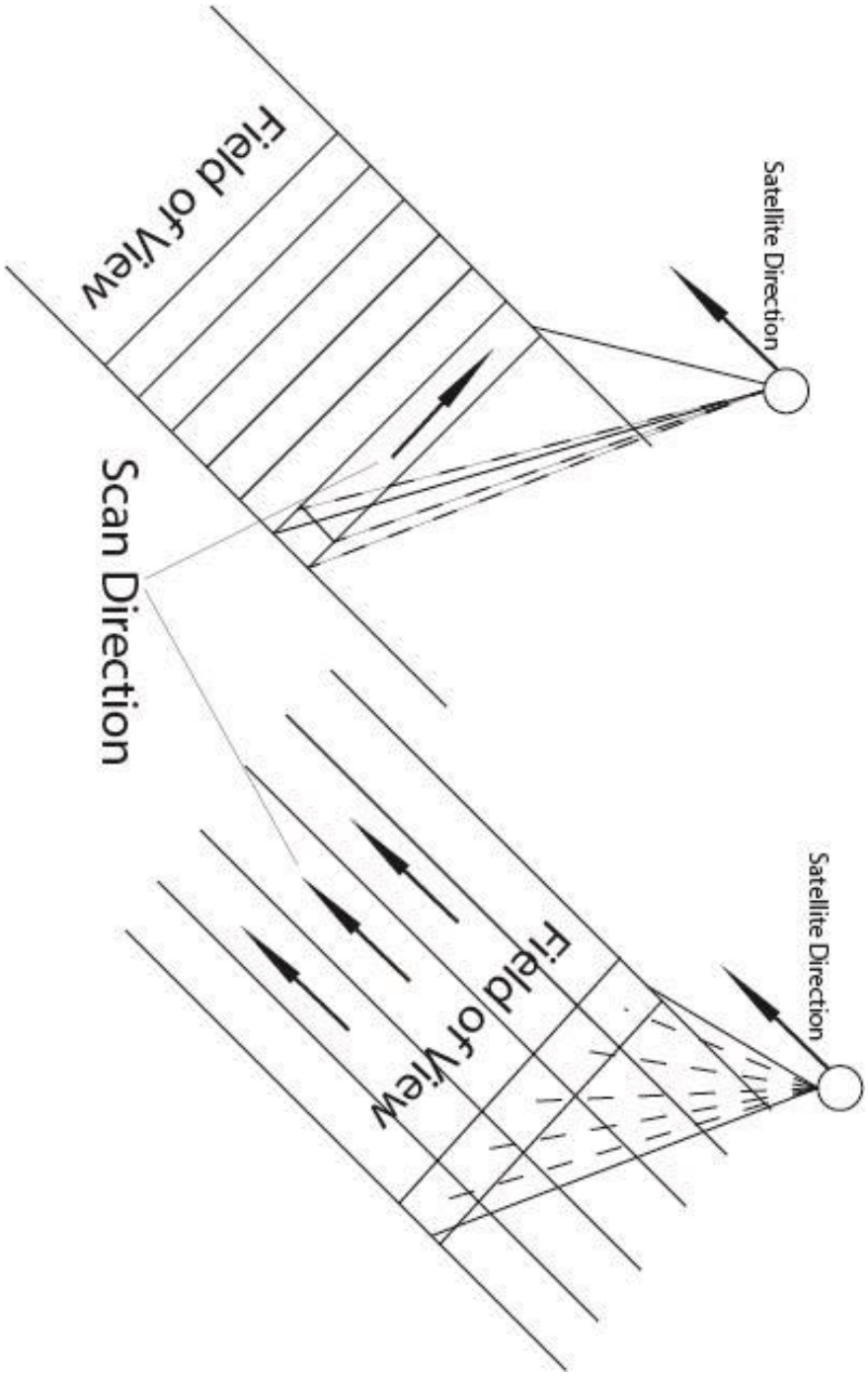

Figure 4. The ability to identify an object on the ground depends on the object size relative to pixel size.

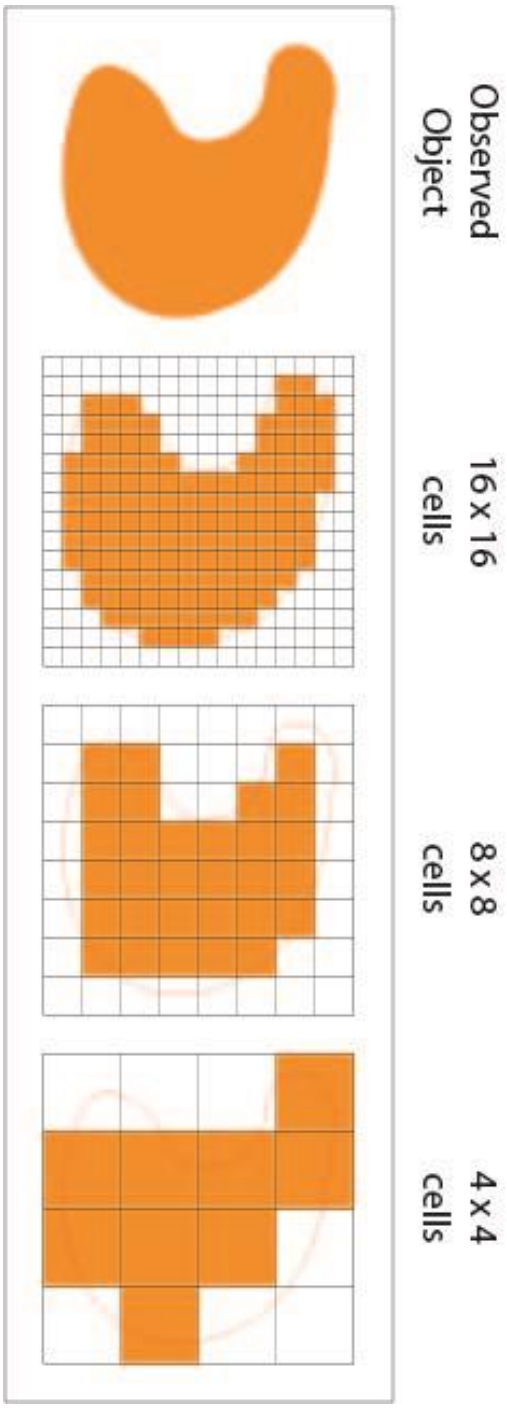

Figure 5. Spectral (a) and radiometric (b) resolutions, represented by the thick green bands and thin red bands for low and high resolutions, respectively. The area under the curve represents the magnitude of electromagnetic energy at various wavelengths. For spectral resolution, low resolution on-board sensors record energy within wide wavelength bands, relative to high resolution sensors. For radiometric resolution, on-board sensors with low resolution are able to detect only large differences in energy magnitude, relative to high resolution sensors.

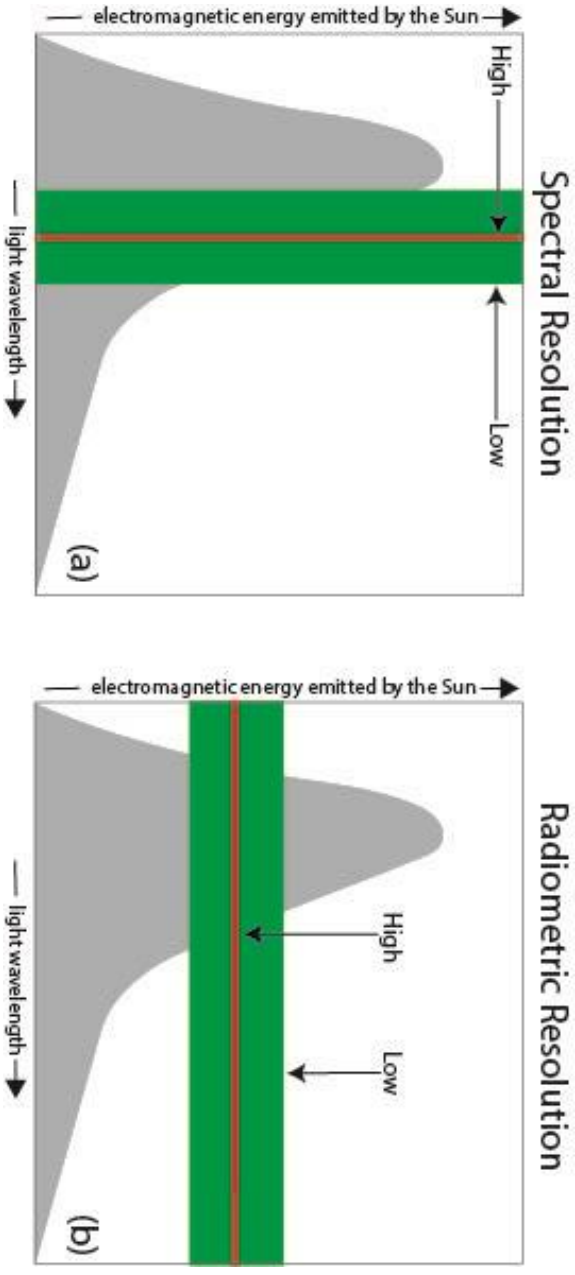

Figure 6. Near Polar and Geostationary Orbits.

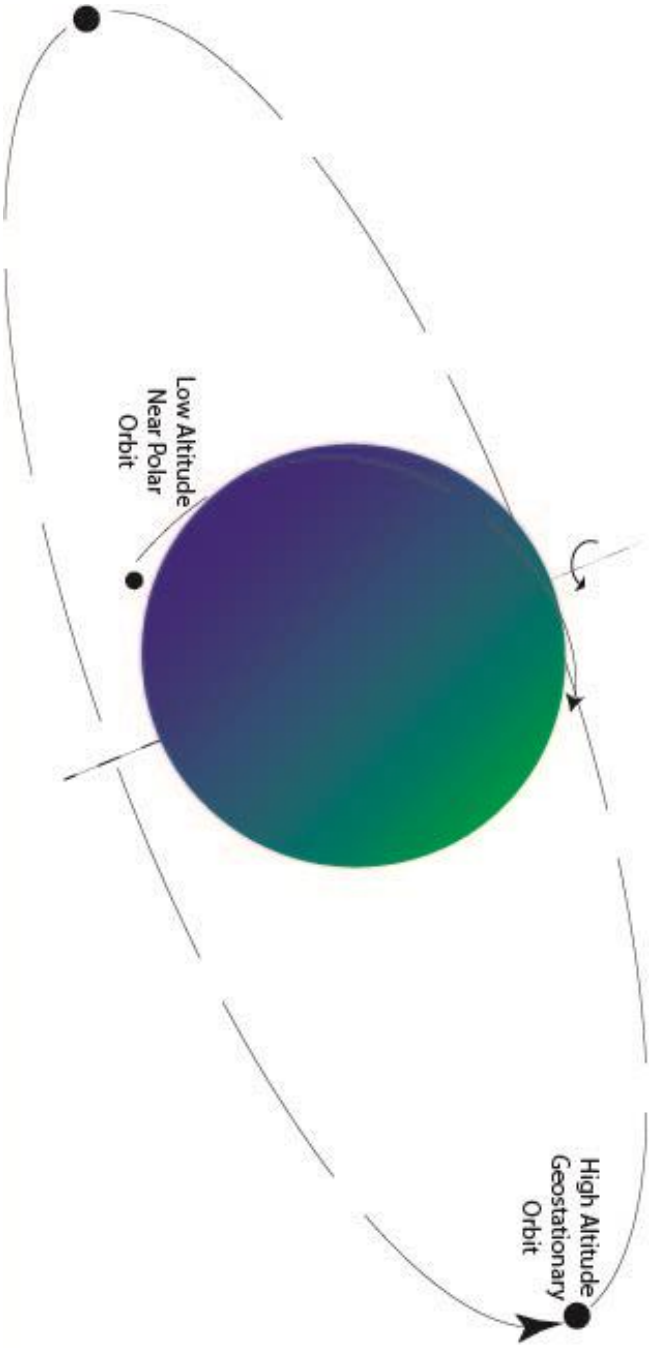

Figure 7. Natural Color Image at 1:5000 scale. Unprocessed, natural color, composite band (top half) with 30 m pixel spatial resolution for an L8 scene abutted against the pansharpened version of the same composite image (bottom half) using the 15 m pixel spatial resolution obtained from the panchromatic band. The undesired color alteration of the spectral information is obvious. Image scene is from L8, path 15/row 35, captured 18 December 2019. Image processed using ESRI ArcGIS, version 10.6.

Figure 8. Contrast Stretching. Three NIR band images from an L8 scene (scale = 1:70,000). The raw, unstretched and radiometrically low-contrast, image is located at the top-right. The max-min stretched image (top-middle) and the standard deviation stretched image (top-left) have the idealized histogram stretching transformation process below the respective images. DN (digital number) = radiometric resolution; sd (standard deviation) is of undefined value for the idealized histograms. Image processed using ESRI ArcGIS, version 10.6. Image scene is from L8, path 15/row 35, captured 18 December 2019. Image processed using ESRI ArcGIS, version 10.6. Histogram images edited from **Jensen, 2016**.

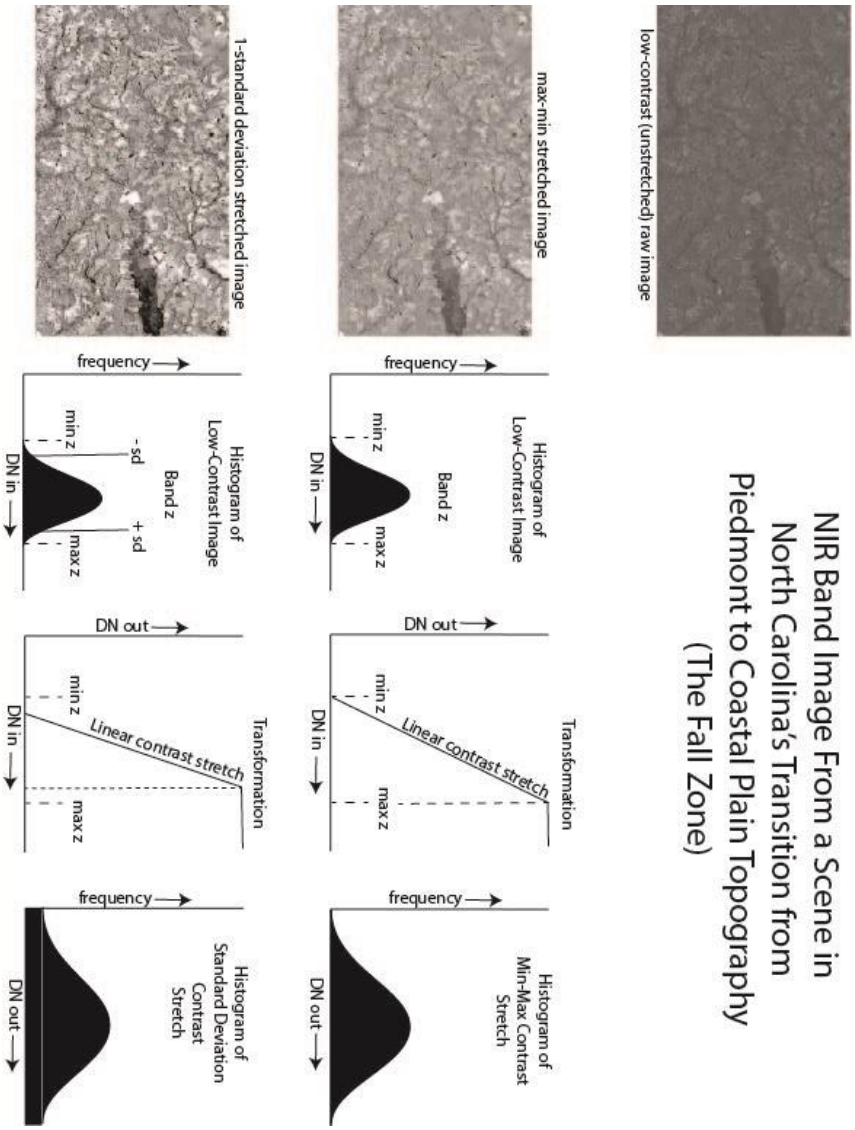

Figure 9. "Sliding Window" Filter Concept. The neighborhood pixels (shaded green) contain the pixel of interest at the center (outlined in red). The numbers in the center grid represent a hypothetical DN value for that pixel in an image raster. In this 3 x 3 neighborhood sub-grid, a simple algorithm possibility for a low-pass (smoothing) function might be to apply a mean value of the neighborhood pixels to the pixel of interest. After the transformation, the value of the center pixel here will become 2. Then, the neighborhood will shift one pixel and repeat the process for the next pixel (from top grid, to center grid, to grid on bottom). In order to accentuate differences in the image, a high-pass (edge detection) function might apply a positive multiplier to the cell of interest, while applying a negative multiplier to the neighborhood pixels.

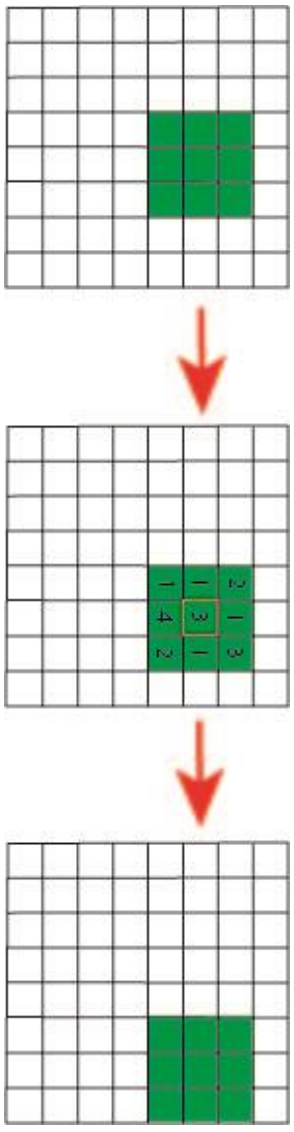

Figure 10. Common Band Assignments for Geology. Natural color image (top-left) and infrared (vegetation-emphasized) image (bottom-left) are the same scene at 1:24000 spatial resolution (see main text for band assignment explanation). The bottom-right scene is centered on the Atlantic fall zone rapids at Roanoke Lake and the Roanoke River, at the town of Roanoke Rapids, North Carolina (spatial resolution is 1:12500) – the pink lineation separating the lake from the river, down-gradient, is the concrete material composing the dam spillway, whereas the blue color patches are metamorphic boulders of the Atlantic fall zone. The high-resolution orthoimagery (top-right) is the featured area circled in magenta from the image below (bottom-right). Having an idea of what to expect on the surface is crucial to geological image interpretation. Image scene is from L8, path 15/row 35, captured 18 December 2019. Image processed using ESRI ArcGIS, version 10.6. High resolution orthophoto was captured 13 February 2011.

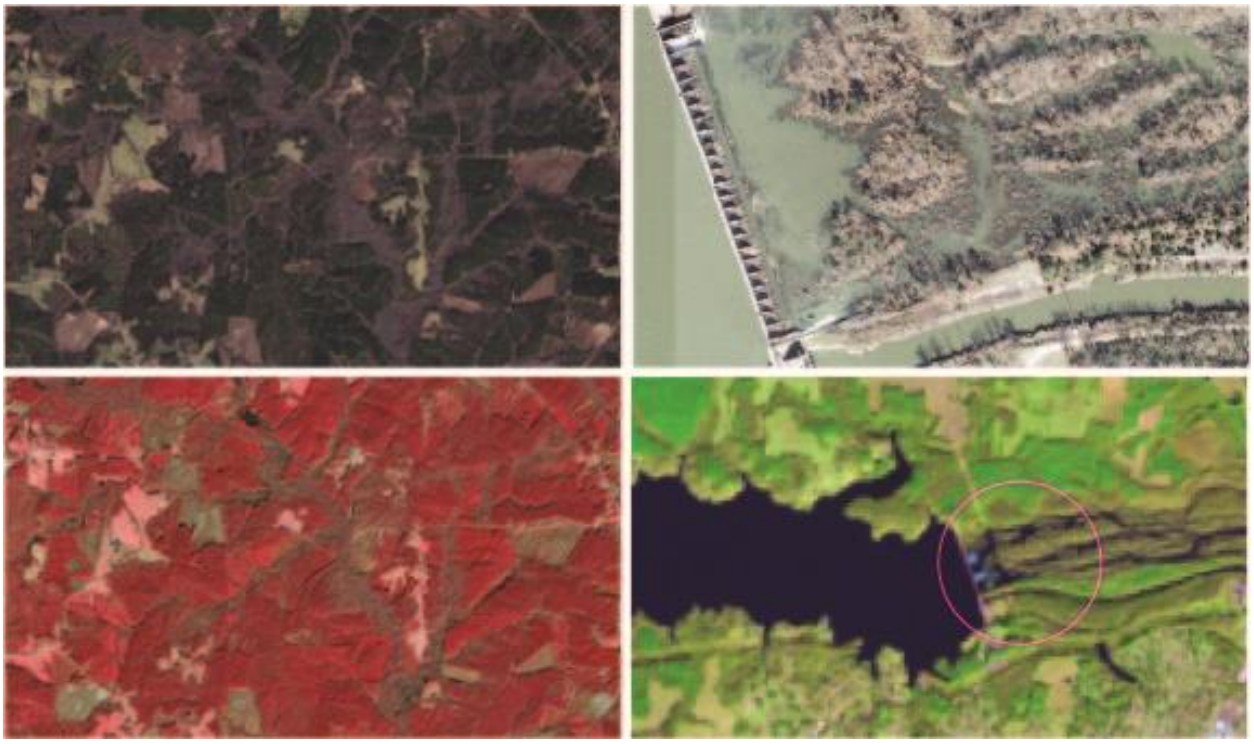

Figure 11. (Middle) Assigning R-G-B to band ratios (visible red / visible green), (SWIR1) / (SWIR2), and (SWIR1) / (NIR), respectively (see **table 3**) manifests the above pattern (scale is 1:24,000 and pixel spatial resolution is 30 m). The magenta patterns should be further investigated for iron-oxide dominated material, light green patterns are potentially dominated by hydroxyl-bearing and clay material, and the blue is possibly iron-rich aluminum silicate material or sand – iron and aluminum are often silica sand impurities (**Boussaa, et al., 2017**). The darker green patterns are heavily vegetated or forested areas. (Left) Natural color image of the scene section. (Right) Lithology map of scene section (**Weems et al., 2009**), where the lithology in the scene is described as: Qchs = (Chuckatuck Fm) sand, containing 1-2% heavy minerals; Qsh = (Shirley Fm) clayey sand; Qal = (Holocene alluvium) coarse-grained sand; Qch = (Chuckagtuck Fm, upper sands) very fine/fine sand; Qt = (Tabb Fm) very fine/fine sand. (See **Weems et al., 2009**; and **Weems and Lewis, 2007** for full lithology descriptions.) Image scene is from L8, path 15/row 35, captured 18 December 2019. Image processed using ESRI ArcGIS, version 10.6.

Figure 12. Conceptual PCA Model of Two-Band Raster. A scatter plot of pixel data from two spectral bands is considered where the points represent the radiometric value (DN) for pixels in the two bands. In any plotting function, the points will be bound by an ellipse (left frame). The major axis of the ellipse is determined and becomes the new x-axis (x'), which has the greatest variation within the scatter plot; this is the first PC (PC1). The direction of PC1 is the eigenvector and its magnitude is the eigenvalue. The angle of the x-axis to PC1 is the angle of rotation used in the transformation (center frame). An orthogonal line perpendicular to PC1 is then produced. This line is the second PC (PC2) and the new y-axis (y') (right frame). PC2 describes the greatest variance not described by PC1 (**Lillesand et al., 2015**).

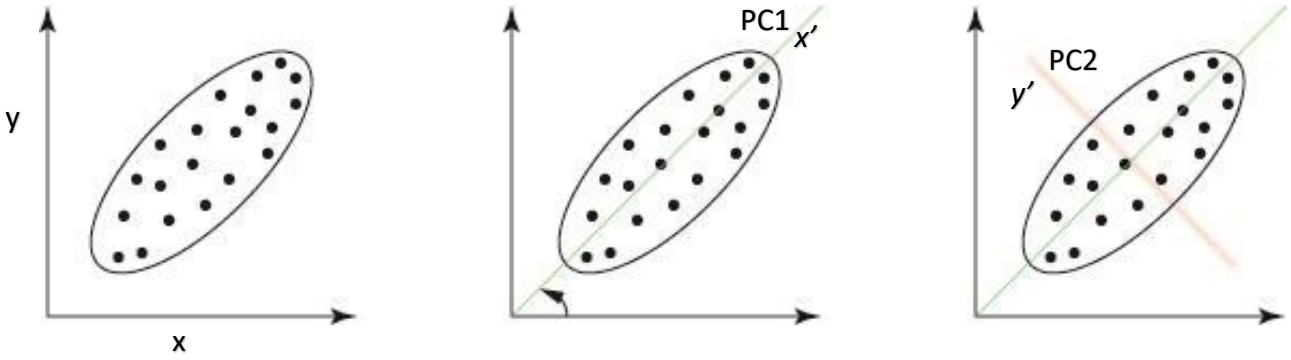

Figure 13. PCA of an image scene covering the Roanoke Rapids, North Carolina 30' x 60' quadrangle. Spectral Bands 2-7 from an L8 scene are used to create the statistical matrices. On the bottom-right, the rows labeled "Input Layer" are the spectral bands, whereas the columns are the PCs. Considering that the first PC is usually directly correlated to the brightness of the original spectral band (**Estornell et al., 2013**), we see in the second PC that there is maximum contrast between the NIR and SWIR2 bands. Using these spectral bands in combinations is likely to be advantageous.

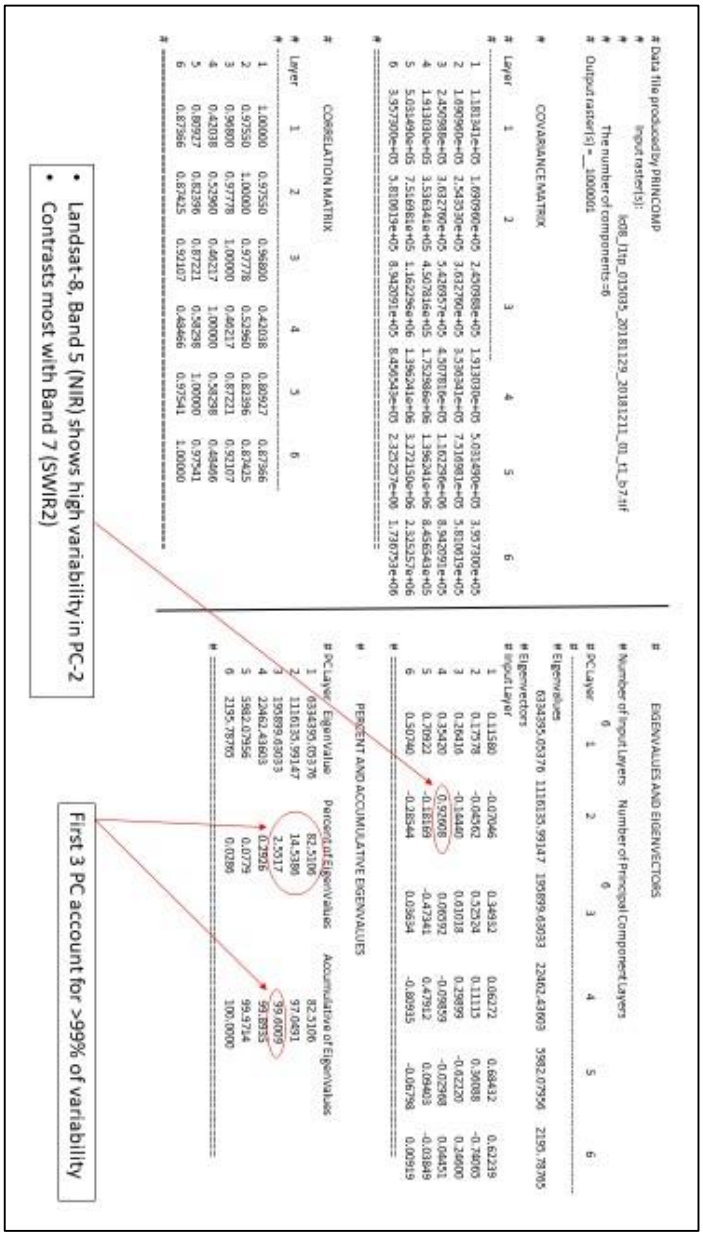

Figure 14. PCA of the Roanoke Rapids, North Carolina 30' x 60' quadrangle. PCAs can look very similar to spectral band combinations when applied for visual analysis. When observing the first component only (top) a gray scale is applied (black = minimum contrast; white = maximum contrast) – although a color ramp can certainly be applied. When R-G-B is assigned to the first three PCs, respectively (bottom), the spectral contrast concentrations are visually displayed from another perspective.

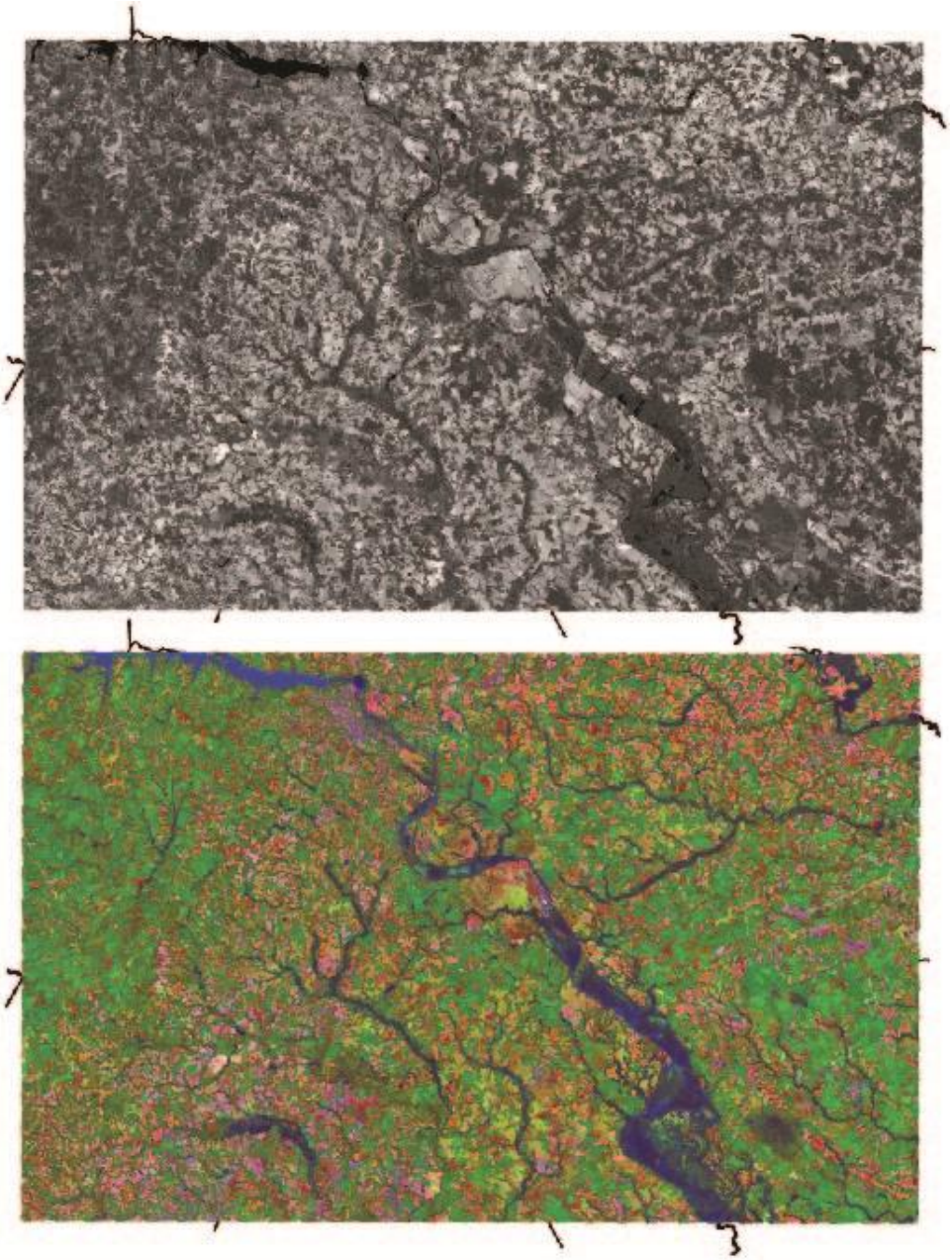

TABLES

Table 1. Landsat 8 (L8) parameters.

Landsat 8			
	Description	**Light Wavelength (nm)**	**Spatial Resolution (m)**
Band 1	Aerosol	430-450	30
Band 2	Blue - visible range	450-510	30
Band 3	Green - visible range	530-590	30
Band 4	Red - visible range	640-670	30
Band 5	NIR	850-880	30
Band 6	SWIR-1	1.57-1.65 (x 10^3)	30
Band 7	SWIR-2	2.11-2.29 (x 10^3)	30
Band 8	Panchromatic	500-680	15
Band 9	Cirrus	1.36-1.38 (x 10^3)	30
Band 10	TIRS-1	10.6-11.19 (x 10^3)	100
Band 11	TIRS-2	11.5-12.51 (x 10^3)	100
Notes: The Landsat documentation does not assign numbers to the SWIR or TIRS bands, numbers are added here for clarification; light wavelength given as a range. **NIR (near-infrared)**. (**USGS, 2019**)			

Table 2. Sentinel-2 (S2) parameters.

Sentinel-2			
	Description	**Light Wavelength (nm)**	**Spatial Resolution (m)**
Band 1	Aerosol	443	60
Band 2	Blue - visible range	490	10
Band 3	Green - visible range	560	10
Band 4	Red - visible range	665	10
Band 5	VNIR-1	705	20
Band 6	VNIR-2	740	20
Band 7	VNIR-3	783	20
Band 8	VNIR-4	842	10
Band 8A	VNIR-5	865	20
Band 9	SWIR-1	940	60
Band 10	Cirrus	1.375 (x 10^3)	60
Band 11	SWIR-3	1.61 (x 10^3)	20
Band 12	SWIR-4	2.19 (x 10^3)	20
Note: The Sentinel documentation does not assign numbers to the VNIR or SWIR bands, numbers are added here for clarification; light wavelength given by central value. (**ESA, 2015**)			

Table 3. Some common Landsat 8 (L8) spectral band ratios useful to geological applications.

Band (B) Ratios	Uses	Detailed Methods Descriptions
(visible red) / (visible blue) OR (B4) / (B2)	Iron oxide	**Segal, 1982**; **Drury, 1987**
(SWIR1) / (visible blue) OR (B6) / (B2)	Magnetite (Fe^{+2} & Fe^{+3}) content	**Sultan et al., 1987**
(SWIR1) / (SWIR2) OR (B6) / (B7)	Hydroxyl-bearing & clay minerals	**Drury, 1987**
(SWIR1) / (NIR) OR (B6) / (B5)	Fe-rich aluminum silicate minerals	**Segal, 1982**; **Drury, 1987**
Note: The similar S2 derived ratios can be constructed using the information from **table 2**.		